Behavioral/Cognitive

40 Hz Steady-State Response in Human Auditory Cortex Is Shaped by Gabaergic Neuronal Inhibition

Alessandro Toso,[1]* Annika P. Wermuth,[1]* Ayelet Arazi,[1] Anke Braun,[2] Tineke Grent-'t Jong,[3,4] Peter J. Uhlhaas,[3,4] and Tobias H. Donner[1]

[1]Section Computational Cognitive Neuroscience, Department of Neurophysiology and Pathophysiology, University Medical Center Hamburg- Eppendorf, Hamburg 20251, Germany, [2]Department of Psychiatry, Charité Universitätsmedizin, Berlin 10117, Germany, [3]Institute of Neuroscience and Psychology, University of Glasgow, Glasgow G12 8QB, United Kingdom, and [4]Department of Child and Adolescent Psychiatry, Charité Universitätsmedizin, Berlin 13353, Germany

The 40 Hz auditory steady-state response (ASSR), an oscillatory brain response to periodically modulated auditory stimuli, is a promising, noninvasive physiological biomarker for schizophrenia and related neuropsychiatric disorders. The 40 Hz ASSR might be amplified by synaptic interactions in cortical circuits, which are, in turn, disturbed in neuropsychiatric disorders. Here, we tested whether the 40 Hz ASSR in the human auditory cortex depends on two key synaptic components of neuronal interactions within cortical circuits: excitation via N-methyl-aspartate glutamate (NMDA) receptors and inhibition via gamma-amino-butyric acid (GABA) receptors. We combined magnetoencephalography (MEG) recordings with placebo-controlled, low-dose pharmacological interventions in the same healthy human participants (13 males, 7 females). All participants exhibited a robust 40 Hz ASSR in auditory cortices, especially in the right hemisphere, under a placebo. The $GABA_A$ receptor–agonist lorazepam increased the amplitude of the 40 Hz ASSR, while no effect was detectable under the NMDA blocker memantine. Our findings indicate that the 40 Hz ASSR in the auditory cortex involves synaptic (and likely intracortical) inhibition via the $GABA_A$ receptor, thus highlighting its utility as a mechanistic signature of cortical circuit dysfunctions involving GABAergic inhibition.

Key words: ASSR; auditory cortex; GABA; humans; MEG; NMDA

Significance Statement

The 40 Hz auditory steady-state response is a candidate noninvasive biomarker for schizophrenia and related neuropsychiatric disorders. Yet, the understanding of the synaptic basis of this neurophysiological signature in humans has remained incomplete. We combined magnetoencephalography (MEG) recordings with placebo-controlled pharmacological interventions in healthy human subjects to test the modulation of the 40 Hz ASSR in the auditory cortex by two synaptic components that have been implicated in the generation of neuronal oscillations in cortical microcircuits: glutamate N-methyl-aspartate glutamate (NMDA) receptors and gamma-amino-butyric acid (GABA) A receptors. Boosting GABAergic transmission, but not blocking NMDA receptors, increased the amplitude of this ASSR. Thus, GABAergic inhibition modulates 40 Hz steady-state responses in the auditory cortex.

Introduction

An important objective of current translational research is the identification of biomarkers of the neural circuit dysfunctions underlying schizophrenia and related disorders, such as autism spectrum disorders. The auditory steady-state response (ASSR), an oscillatory brain response to a periodically modulated auditory stimulus, has recently gained attention as a candidate neurophysiological biomarker of schizophrenia (Grent-'t-Jong et al., 2023).

The ASSR can be measured noninvasively via electroencephalography (EEG) or magnetoencephalography (MEG; Tan et al., 2015; Thune et al., 2016). The ASSR peak frequency occurs at stimulus frequencies ~40 Hz (Galambos et al., 1981; Pastor et al., 2002), pointing to a resonance property of the stimulus-driven neural circuits. A substantial body of evidence indicates a reduction of the 40 Hz ASSR in patients diagnosed with schizophrenia (SCZ; Kwon et al., 1999; Tan et al., 2015; Tada et al., 2021; Onitsuka et al., 2022) as well as in individuals at risk of developing the disorder (Grent-'t-Jong et al., 2021; Tada et al., 2021) and first-degree relatives of schizophrenia patients (Hong et al., 2004; Rass et al., 2012). A reduction of the 40 Hz ASSR has also been reported in bipolar disorder (Jefsen et al., 2022) and autism (Wilson et al., 2007).

Developing a mechanistic understanding of the 40 Hz ASSR requires delineating the synaptic basis of the 40 Hz ASSR. As a response to an oscillatory stimulus input to the brain, the ASSR may, in principle, simply result from the linear superposition of a sequence of auditory evoked potentials that are faithfully propagated from the inner ear to the auditory cortex (Galambos et al., 1981; Ozdamar et al., 2007; Bohorquez and Ozdamar, 2008; Presacco et al., 2010). However, some evidence indicates that cortical circuits may amplify ASSRs specifically around the 40 Hz range through intrinsic, recurrent interactions (Pastor et al., 2002; Ross et al., 2002). Stimulus-induced gamma-band (40–80 Hz) oscillations result from the reciprocal interaction between excitatory pyramidal cells and inhibitory cells (Donner and Siegel, 2011; Buzsaki and Wang, 2012), with an important role of gamma-amino-butyric acid (GABAergic) inhibitory interneurons (Cardin et al., 2009; Sohal et al., 2009; Veit et al., 2017) and glutamatergic N-methyl-aspartate (NMDA) receptor–mediated drive of those interneurons from pyramidal neurons (Carlen et al., 2012; Jadi et al., 2016).

The goal of the current study was to determine whether NMDA and GABA$_A$ receptors are also involved in the generation of 40 Hz ASSRs. To this end, we performed MEG recordings of 40 Hz ASSRs under placebo-controlled pharmacological manipulation of both, GABA$_A$ and NMDA receptors in the same participants. We found a marked increase of 40 Hz ASSRs in the auditory cortex under GABA$_A$ receptor stimulation, but not under NMDA receptor blockade.

Material and Methods

Participants
Twenty-three healthy human participants (mean age, 28; range, 21–40, nine females) took part in the study after informed consent and introduction to the experimental procedure. The study was approved by the ethics review board of the Hamburg Medical Association responsible for the University Medical Center Hamburg–Eppendorf (UKE). Exclusion criteria, all of which were assessed by self-report, were: history of any neurological or psychiatry disorders, hearing disorder, history of any liver or kidney disease or metabolic impairment, history of any chronic respiratory disease (e.g., asthma), history of hyperthyroidism or hypothyroidism, pheochromocytoma (present or in history), allergy to medication, known hypersensitivity to memantine or lorazepam, family history of epilepsy (first or second degree relatives), family history of psychiatric disorders (first or second degree relatives), established or potential pregnancy, claustrophobia, implanted medical devices (e.g., pacemaker, insulin pump, aneurysm clip, electrical stimulator for nerves or brain, intracardiac lines), any nonremovable metal accessories on or inside the body, having impaired temperature sensation and/or increased sensitivity to heat implants, foreign objects and metal in and around the body that are not MRI compatible, refusal to receive information about accidental findings in structural MR images, hemophilia,

frequent and severe headaches, dizziness, or fainting, and regularly taking medication or have taken medication within the past 2 months.

Three participants were excluded from the analyses: one due to excessive MEG artifacts and the other two due to not completing all six recording sessions. Thus, we report the results from $n = 20$ participants (seven females). The sample size was based on the common sample sizes used in human MEG studies.

Participants were remunerated 15 Euros for the behavioral training session, 100 Euros for each MEG session, 150 Euros for completing all six sessions, and a variable bonus, the amount of which depended on task performance across all three sessions. The maximum bonus was 150 Euros.

Experimental design
Each participant completed six experimental sessions, each starting with the oral intake of a pill (see below). During MEG, participants were seated on a chair inside a magnetically shielded chamber. Each MEG session was ~2.5 h in duration and consisted of different tasks including the ASSR task described below. The ASSR task took place usually ~90 min after the start of the MEG recording (i.e., 4 h after drug intake).

Pharmacological intervention. In each of the six experimental sessions, we administered one of two drugs or a placebo (double-blind, randomized, crossover design): the NMDA receptor antagonist memantine (Johnson and Kotermanski, 2006), the GABA$_A$ receptor agonist lorazepam (Kienitz et al., 2022), or a mannitol–aerosil placebo. Both drugs and the placebo were administered during two (randomly selected) sessions. The dosages were 15 mg for memantine (clinical steady-state dose for adults, 20 mg) and 1 mg for lorazepam (common clinical daily dose between 0.5 and 2 mg). The substances were encapsulated identically to render them visually indistinguishable. Participants received the pill 150 min before the start of MEG recordings. This delay was chosen to jointly maximize plasma concentrations of both drugs during MEG recordings (spanning ~2 h): peak plasma concentrations are reached ~3–8 h after memantine administration (Noetzli and Eap, 2013) and 2–3 h after lorazepam administration (Greenblatt et al., 1982). Participants were kept under observation during the waiting period following administration of the pill, and their blood pressure and heart rate were recorded every 15 min. The first and senior authors are both certified medical doctors, and emergency medical care by the University Medical Center Hamburg–Eppendorf was available on campus at any time. The six sessions were scheduled at least 1 week apart to allow plasma levels to return to baseline [plasma half-life of memantine: ~60–70 h (Noetzli and Eap, 2013); half-life of lorazepam: ~13 h (Greenblatt et al., 1982)].

Stimulus and task. During the ASSR task in the MEG, we presented 100 repetitions of 1,000 Hz carrier tones (duration: 2 s) that were amplitude modulated (ripple tones) at 40 Hz (Tan et al., 2015). In a subset of sessions, the stimulus was amplitude modulated (AM) at 36.75 Hz ($n = 33$ over 125 sessions), enabling us to establish the stimulus–frequency dependence. Stimuli were presented binaurally through inner ear tubes with an interstimulus interval of on average 2 s (jittered between 1.5 and 2.5 s, equal distribution). Ten flat tones (the same intensity as ripple tones) were randomly intermixed with the ripple tones. Participants were instructed to fixate on a translucent screen (viewing distance, 64 cm) and respond to the flat tones via button press. These trials were not included in the MEG analyses. Auditory stimuli were presented at a fixed pressure level of 70 dB in both ears for all sessions.

Data acquisition
MEG. We used a CTF MEG system with 275 axial gradiometer sensors and recorded at 1,200 Hz, with a (hardware) antialiasing low-pass filter (cutoff, 300 Hz). Recordings took place in a dimly lit magnetically shielded room. We concurrently collected eye-position data with a SR-Research EyeLink 1000 eye-tracker (1,000 Hz). We continuously monitored the head position by using three fiducial coils. After seating the participant in the MEG chair, we created and stored a template head position. At the beginning of each following session and after each block, we guided participants back into this template position.

We used Ag/AgCl electrodes to measure ECG and vertical and horizontal EOG.

Magnetic resonance imaging. Structural T1-weighted magnetization prepared gradient-echo images (TR = 2,300 ms, TE = 2.98 ms, FoV = 256 mm, 1 mm slice thickness, TI = 1,100 ms, 9° flip angle) with $1 \times 1 \times 1$ mm^3 voxel resolution were obtained on a 3 T Siemens Magnetom Trio MRI scanner (Siemens Medical Systems). Fiducials (nasion, left and right intra-aural point) were marked on the MRI.

Data analysis

MEG data were analyzed with a combination of customized scripts (https://github.com/Tosot91/ASSR_MEG_drugs.git) and the following toolboxes: FieldTrip (Oostenveld et al., 2011) version 20201009 for MATLAB (2021a; MathWorks) as well as MNE (Gramfort et al., 2013) and pymeg for Python (https://github.com/DonnerLab/pymeg) established in a previous work from our laboratory (Wilming et al., 2020).

Behavior. For the quantification of task behavior, we analyzed hit rate (percentage of correctly detected flat-tone targets), false alarm rate (percentage of ripple tones incorrectly reported as target flat tones), and reaction times.

Preprocessing. We used an automated algorithm to label artifacts in the continuous time series recorded in each session. Sensor jumps were detected by convolving each sensor with a filter designed to detect large sudden jumps and subsequently by looking for outliers in the filter response. Muscle and environmental artifacts (e.g., cars passing by the vicinity of the MEG room) were detected by filtering each channel in the 100–140 Hz or <1 Hz range and by detecting outliers that occurred simultaneously in many channels. After removing epochs containing head movements, squid jumps and muscle artifacts, the remaining time series were then subjected to temporal independent component analysis (infomax algorithm), and components containing blink or heartbeat artifacts were identified manually and removed. We applied a notch filter to remove 50 Hz power line noise and its harmonics (100–150 Hz) and a high-pass linear phase FIR filter (order 3) with a cutoff frequency of 0.1 Hz. The resulting data were segmented in trial epochs of 3 s duration (0.5 s baseline) time-locked to sound onset and all epochs that contained artifacts as defined above were discarded. Finally, the preprocessed data were downsampled to a sampling rate of 400 Hz. For subsequent sensor-level analyses, the MEG data were first submitted to a planar gradient transformation (Bastiaansen and Knosche, 2000).

Spectral analysis. The preprocessed data from each sensor were then submitted to spectral analysis using sliding-window Fourier transform (Welch's method, Hanning tapered; padding, 4 s) with a frequency resolution of 0.25 Hz, window length of 500 ms, and step size of 25 ms. For sensor-level analyses, spectral power was then computed, for each time and frequency bin, by taking the absolute value of the (complex-valued) Fourier coefficients and squaring. The ASSR was evaluated by normalizing the power at each time and frequency bin (for topographies and cortical maps: time-averaged power at the stimulus frequency ±1 Hz) with the power in the prestimulus baseline interval (averaged across trials and time in the interval −250 to 0 ms before stimulus onset). The stimulus-phase–locked component of the ASSR was evaluated by first averaging the broadband MEG signal across trials in the time domain, followed by spectral analysis and baseline normalization as described above (Donner and Siegel, 2011). Intertrial phase coherence (ITPC) was computed for each frequency (f) and time window (t) as follows:

$$\text{ITPC}(f, t) = \frac{1}{N} \sum_{k=1}^{n} \frac{F_k(f, t)}{|F_k(f, t)|},$$

where F denotes the Fourier transform, k is the trial number, and $||$ is the complex norm. ITPC ranges from 0 (random phases across trials) to 1 (perfect phase alignment across trials).

Source reconstruction. We used linearly constrained minimum variance (LCMV) beamforming (Van Veen et al., 1997) to project the MEG data into source space. To this end, we constructed individual three-layer head models (inner skull, outer skull, and skin) from each subject's structural MRI scans. These head models were aligned to the MEG data by a transformation matrix that aligned the average fiducial coil position in the MEG data and the corresponding locations in each head model. Transformation matrices were then generated. We computed one transformation matrix per recording session. We then reconstructed individual cortical surfaces from the structural MRIs and aligned the Glasser atlas (Glasser et al., 2016) to each surface. Based on the head model, we generated a forward model ("leadfields") for the computation of LCMV filters that was confined to the cortical sheet (4,096 vertices per hemisphere, recursively subdivided octahedron). To compute the LCMV filter for each vertex, the leadfield matrix for that vertex was combined with the trial-averaged covariance matrix of the (cleaned and epoched) data estimated for the stimulus interval (0–2 s from stimulus onset). We chose the source orientation with maximum output source power at each cortical location. We projected the broadband time series into source space and then extracted power (taking absolute value and squaring) for each frequency and time bin. The power values were extracted at each vertex and finally averaged across all vertices within a given region of interest (see the next section).

Regions of interest (ROIs). We used an established anatomical parcellation of the human cortical surface to define ROIs for further analysis (Glasser et al., 2016). For computing cortex-wide maps of the ASSR, the baseline-normalized power response at the stimulus frequency (±1 Hz) for the interval from 0.1 to 2 s from stimulus onset was estimated for all 360 parcels of the above atlas. All other analyses collapsed across, the bilateral "early auditory cortex" group, which consists of the following five areas per hemisphere [Glasser et al., 2016; A1, lateral belt (LBelt), medial belt (MBelt), para-belt (PBelt), and retroinsular cortex (RI)]. We focused our analyses on this area group as our primary, a priori ROI. We refer to this collapsed ROI as "early auditory cortex" in the following. We used the bilateral central dorsolateral prefrontal cortex group (dlPFC; comprising areas, 9–46d, 46, a9–46v, and p9–46v) as the control for anatomical specificity.

Statistical analyses. Sensors showing a significant 40 Hz ASSR were determined using cluster-based permutation tests ($a = 0.05$, two-sided, $n = 10,000$) across all 40 Hz sessions under placebo condition, with baseline (−250 to 0 ms) and stimulus-induced (100–2,000 ms) ASSR power averaged across 39–41 Hz as paired samples. The main effects of stimulation at the source level were determined from source reconstructed ASSR power modulations (expressed in percentage relative to prestimulus baseline power) at stimulus frequency ±1 Hz from all 360 Glasser atlas ROIs, using a permutation test [two-sided, false discovery rate (FDR)-corrected] across all 20 subjects and sessions under placebo condition. Source-level ASSRs from the early auditory cortex (both total and phase-locked power) were also subjected to cluster-based permutation tests across participants ($a = 0.05$, two-sided, $n = 10,000$) to evaluate if drug differences in MEG power or ITC were significantly different from zero) between 0 and 2,250 ms and stimulus frequency ±5 Hz (Figs. 3A, 4A, 5B) and between 0 and 2,250 ms averaged across stimulus frequency ±1 Hz (Figs. 3B, 4B, 5C). Permutation tests were used to evaluate drug differences for the transient component (100–400 ms from stimulus onset and at stimulus frequency ±1 Hz) and the sustained component (650–1,750 ms from stimulus onset and at stimulus frequency ±1 Hz; Figs. 3C, 4C, 5D). The sustained response interval was chosen to avoid any overlap of spectral estimation time windows with the transient or poststimulus intervals.

Results

We recorded MEG responses in 20 healthy participants after administration of the NMDA receptor antagonist memantine, the GABA$_A$ receptor agonist lorazepam, or a glucose placebo (Fig. 1A; see Materials and Methods). Both drugs were applied at relatively low dosages (see Materials and Methods). The ASSR stimuli consisted of 1,000 Hz carrier tones (duration, 2 s)
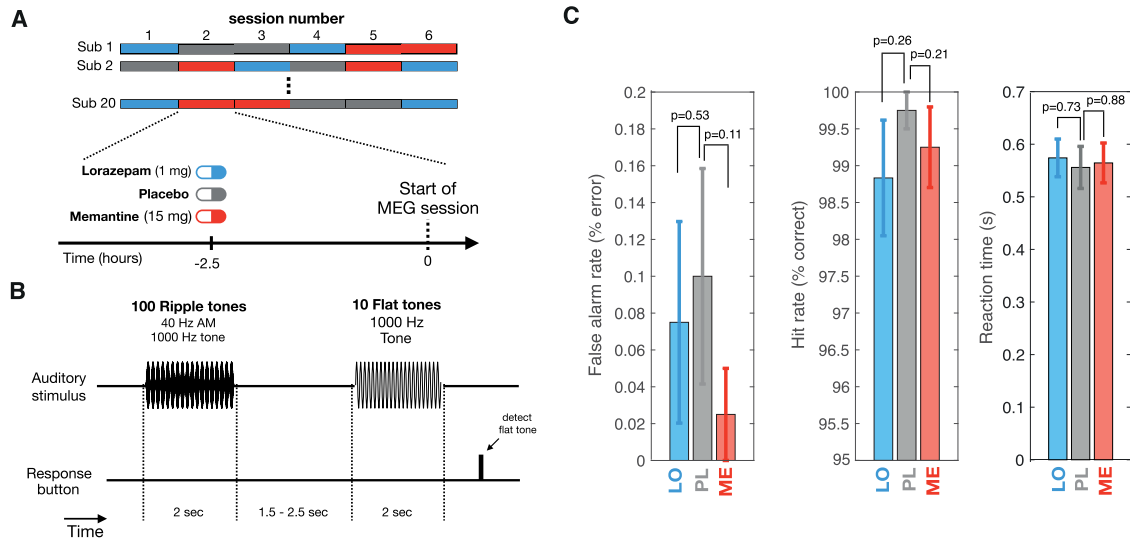
Figure 1. Experimental design, task, and behavior. **A**, Experimental design. Subjects underwent six MEG sessions following intake of placebo, lorazepam, or memantine and a 2.5 h waiting period. See Materials and Methods for details. **B**, ASSR task. Participants had to detect ten 1,000 Hz flat tones interleaved in between 1,000 Hz tones amplitude modulated at 40 Hz (ripple tones). **C**, Behavioral performance for drug conditions. Error bars, SEM. *p*-values obtained from two-sided permutation tests (*N* = 1,000 repetitions) of differences between drug and placebo conditions.

that were amplitude modulated at either 40 Hz or 36.75 Hz and presented binaurally (Fig. 1*B*; Grent-'t-Jong et al., 2021).

Participants were instructed to fixate on a translucent screen and to detect and respond to flat tones (10 in total) that occurred at random times in between the ripple tones with equal intensity levels over time via button press. The flat tones were presented to control attention but were not used for analyses of the MEG data. The drugs did not affect behavior in this task (Fig. 1*C*, see Materials and Methods), with only a small fraction of participants showing a slightly higher false alarm rate and lower hit rate (6 over 20) compared with maximum performance. Thus, differences in effort or general alertness were unlikely causes of any effects on cortical responses reported below.

Spatially and frequency-specific ASSRs

The amplitude-modulated tones produced a robust and specific 40 Hz ASSR during placebo (Fig. 2). This response was evident in sensors overlying the left and right temporal cortex, with a sustained and significant (*p* < 0.01, cluster-based permutation test) increase in 40 Hz power relative to prestimulus interval over 198 right and left frontotemporal sensors (Fig. 2*A*). The 40 Hz ASSR was also evident in source reconstructions centered on bilateral auditory cortices) but also including several further temporal and more distant cortical areas (Fig. 2*B*). The 40 Hz ASSR was stronger in the right hemisphere (Fig. 2*B*), in line with previous works (Ross et al., 2005; Grent-'t-Jong et al., 2021). All our further analyses focused on the bilateral early auditory cortex because this is the first stage of auditory cortical processing and it should (as expected) be the most prominent ASSR. The ASSRs detected in neighboring areas may, at least in part, be due to leakage from the auditor cortex ASSR through the spatial filters used for source reconstruction (Materials and Methods).

When we varied the frequency of the stimulus amplitude modulation (henceforth "stimulus frequency" for brevity) between 40 and 36.75 Hz, the auditory cortex ASSR was strong in both conditions, with a peak frequency that shifted correspondingly in a dependable manner (Fig. 2*C*). In contrast, there was no detectable response in other control regions such as the

dorsolateral prefrontal cortex (Fig. 2*D*). When isolating the phase-locked component of the stimulus response (Materials and Methods; Donner and Siegel, 2011), we found a similarly sustained and frequency-specific, phase-locked component in the early auditory cortex (Fig. 2*E*). Robust ASSRs were detected within each subject (Fig. 2*F*).

In sum, our stimulus protocol and data analysis approach yielded robust, sustained, and lawful ASSRs in the early auditory cortex, with a clear phase-locked component. We next quantified the differences in this ASSR between drug and placebo conditions to assess the involvement of glutamatergic and GABAergic synapses in its generation.

Boosting GABAergic transmission increases the ASSRs in the auditory cortex

Lorazepam increased the 40 Hz ASSR in the early auditory cortex relative to both placebo and memantine, with no detectable effect for memantine versus placebo (Fig. 3*A,B*). Both the early transient response component (100–400 ms from stimulus onset, *p* = 0.015 vs PL, *p* = 0.004 vs ME) and the later sustained component (650–1,750 ms from stimulus onset, *p* = 0.011 vs PL, *p* = 0.009 vs ME) of the ASSR were increased under lorazepam (Fig. 3*C*). Memantine had no detectable effect on the ASSR. We found no statistically significant effect on the phase-locked response component when assessed in isolation (Fig. 4*A,B*), with a significant increase in power under lorazepam only in the early transient, but not the later sustained component of the ASSR (Fig. 4*C*). We also found no statistically significant effect on intertrial phase coherence (ITPC; Fig. 5).

Discussion

To illuminate the synaptic and circuit mechanisms underlying the generation of 40 Hz ASSRs, we performed MEG recordings of ASSRs under placebo-controlled manipulation of both GABA$_A$ and NMDA receptors in human participants. We found that boosting GABAergic transmission through lorazepam robustly increased the 40 Hz ASSR amplitude in the auditory cortex, relative to both placebo and the NMDA receptor
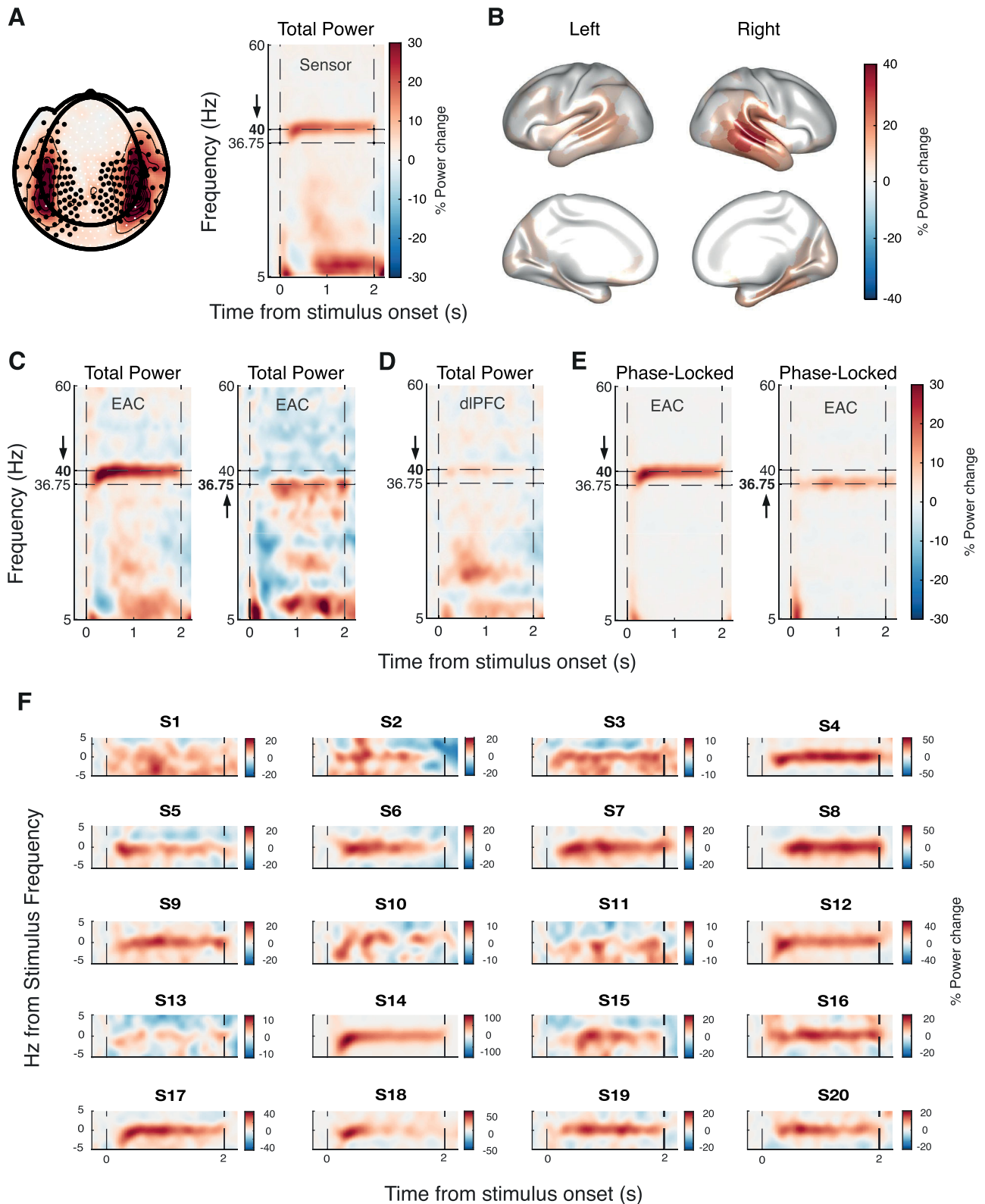
Figure 2. The main effects of ASSR stimulation under placebo conditions. ***A***, Left panel, % Power change relative to the prestimulus interval at sensor-level averaged across 39 to 41 Hz and 100 to 2,000 ms after stimulus onset. Significantly entrained sensors ($p < 0.01$) are marked with black dots. Right panel, Time–frequency representation of average power change relative to the prestimulus interval for significantly entrained sensors. ***B***, Significant increases of 40 Hz power across 360 Glasser atlas ROIs. ***C***, Time–frequency representation of power changes relative to the prestimulus interval in 40 Hz sessions (left panel) and 36.75 Hz sessions (right panel) in the early auditory cortex. ***D***, Same as panel ***C*** but for dlPFC. ***E***, Time–frequency representation of phase-locked signal components in 40 Hz sessions (left panel) and 36.75 Hz sessions (right panel) in EAC. ***F***, Same as panel ***C*** but relative to stimulus frequency and shown separately for each individual (S, subject).
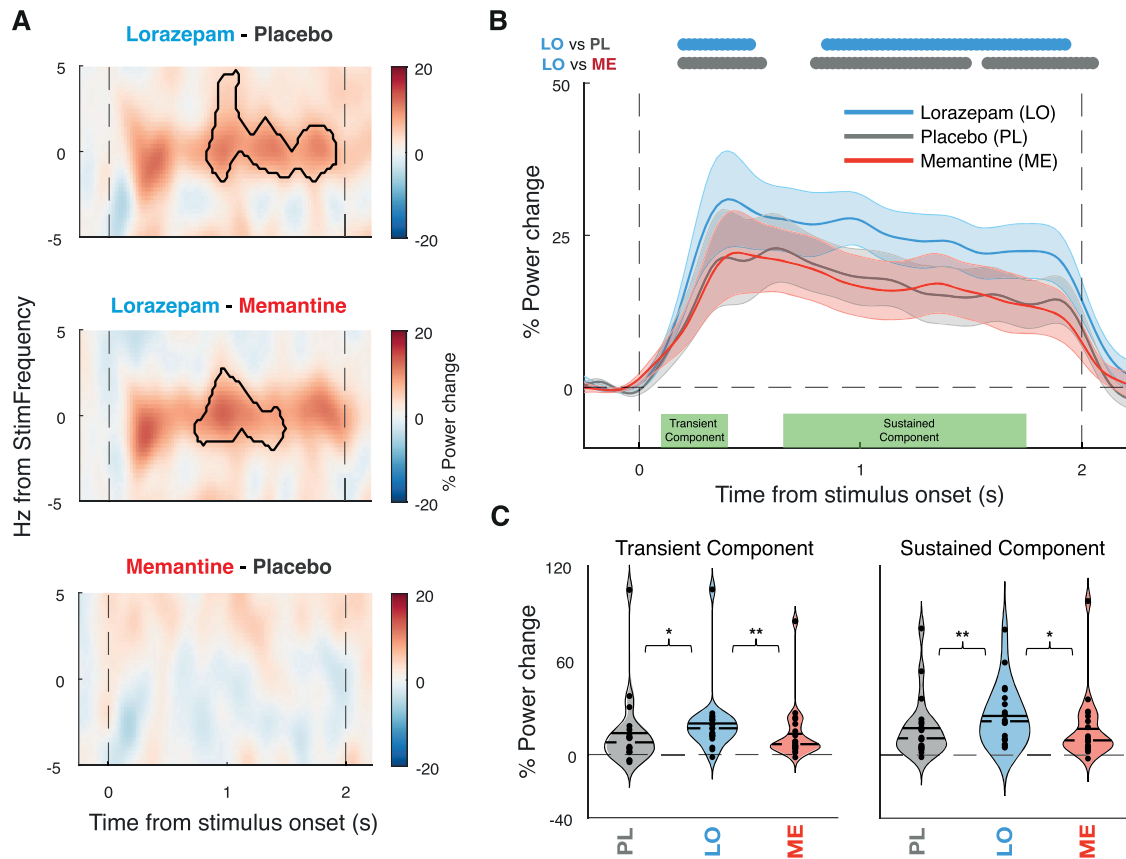
Figure 3. The main drug differences in the auditory steady-state response (ASSR) signals. **A**, Time–frequency representation of the power response in the early auditory cortex shown as percentage power change between drugs. Contour indicating significant differences between drug conditions ($p < 0.05$; cluster-based permutation test). The dashed vertical lines indicate stimulus onset and offset. **B**, Percentage of power change from baseline over time averaged across ± 1 Hz from stimulus frequency for each drug. Horizontal bars, condition differences ($p < 0.05$; cluster-based permutation test), and shaded error bars representing SEM. **C**, % Power change for each drug for stimulus frequency (± 1 Hz), separately for transient (100–400 ms from stimulus onset, left) and sustained (650–1,750 ms from stimulus, right) response components. The sustained response interval was chosen to avoid any overlap of spectral estimation time windows with the transient or poststimulus intervals. The solid line represents the mean, and the dashed line represents the median. Significance estimated via permutation dependent-sample test indicated by stars (*$p < 0.05$, **$p < 0.01$).

antagonist memantine. Our findings are consistent with previous animal work applying other GABAergic drugs and recordings in the hippocampus (Vohs et al., 2010, 2012) or temporal cortex (Yamazaki et al., 2020) and establish a role of GABAergic synaptic transmission in the generation 40 Hz ASSR in human auditory cortex.

Stimulus-evoked, phase-locked responses and response amplification (i.e., resonance) through intrinsic cortical circuit interactions differentially shape the transient and sustained components of cortical power responses (Donner and Siegel, 2011), with early transient response components reflecting predominantly the stimulus-evoked activity and late sustained components reflecting intrinsic circuitry (Ross et al., 2002; Tada et al., 2021; Grent-'t-Jong et al., 2023). Here, we found that the lorazepam effect was evident in both the early and sustained parts of the total spectral power response at 40 Hz (Fig. 3B,C). In contrast, for the phase-locked component of the 40 Hz, the lorazepam effect was only evident in the early, but not the sustained, part of the response (Fig. 4B,C), and no effect was found on intertrial phase coherence (Fig. 5). This is in line with a role of GABAergic circuit interactions in the intrinsic amplification of the ASSR within the early auditory cortex. Such recurrent cortical interactions may introduce small phase jitter that leads to cancellation when averaging across trials in order to isolate the phase-locked component (Donner and Siegel, 2011).

Previous work has shown that the impact of NMDA receptor blockade on 40 Hz ASSRs may vary depending on the type of open channel blocker, dose, or mode of drug administration. Subcutaneous administration of the NMDA-R antagonist ketamine in rodents resulted in an increased ASSR power (Vohs et al., 2012; Munch et al., 2023). Another rodent study using acute intravenous ketamine infusion yielded, likewise, a 40 Hz ASSR amplitude increase at low dosage, but an amplitude reduction at higher dosage (Sivarao et al., 2016), indicating a nonlinear dose–response relationship. Ketamine infusion in humans also yielded a 40 Hz ASSR amplitude increase (Plourde et al., 1997). NMDA receptor blockade via MK-801 in anesthetized rats (Sivarao et al., 2013) or its injections confined to the thalamus (Wang et al., 2020), both decreased the 40 Hz ASSR amplitude, while another study reported an increase in 40 Hz ASSR power when MK-801 was administered intraperitoneally in awake rats (Sullivan et al., 2015). One human EEG study administering memantine found a 40 Hz ASSR increase at frontal electrodes at 20 mg dosage, but no effect at 10 mg (Light et al., 2017). The lack of a detectable memantine effect on the 40 Hz ASSR in the auditory cortex in our current study may, therefore, be due to the lower dosage, the small sample size, the time from ingestion (short relative to memantine kinetics, see Materials and Methods), or a combination of these factors. Future work focussing on NMDA receptor effects could use longer waiting times
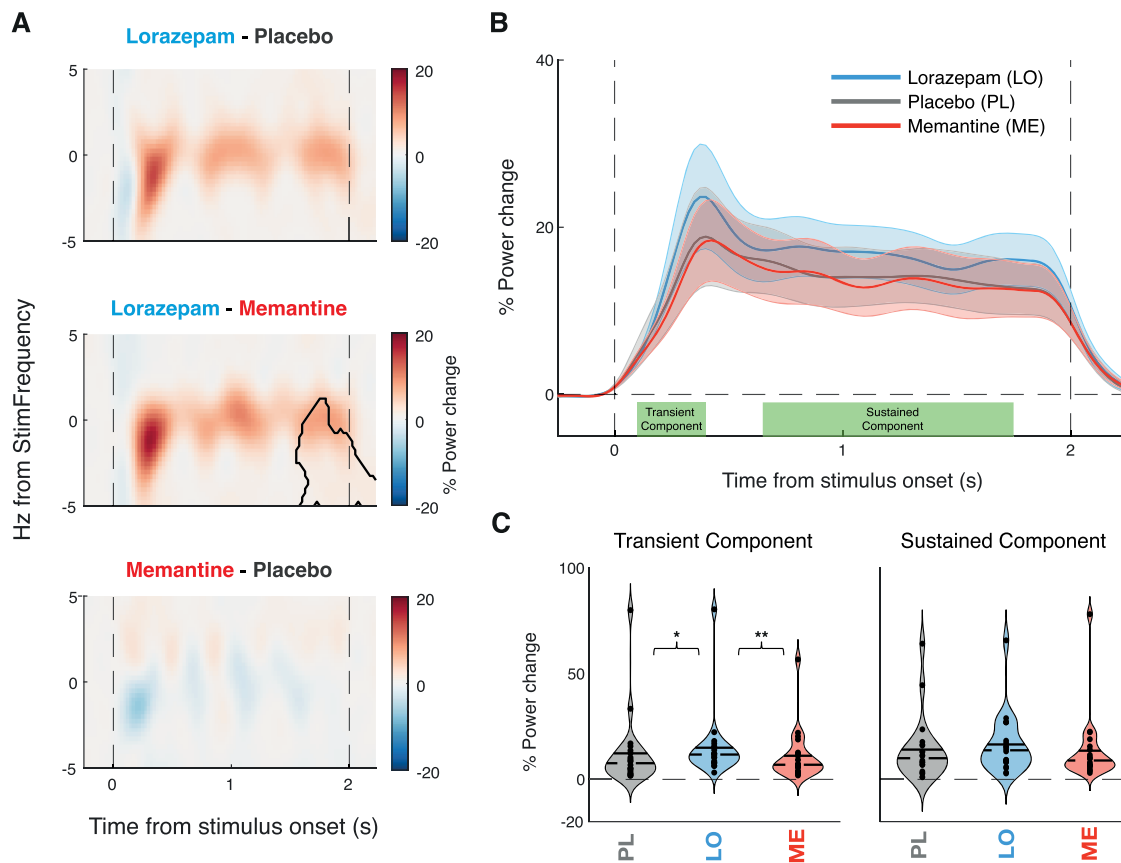
Figure 4. Drug effects on phase-locked response component. ***A***, Time–frequency representation of the power response in the early auditory cortex shown as percentage power change between drugs. Contour indicating significant differences between drug conditions estimated via Monte Carlo cluster-based permutation dependent-sample *t* test. The dashed vertical lines indicate stimulus onset and offset. ***B***, % Power change over time averaged across stimulus frequency ±1 Hz for each drug with dots above indicating significant differences between drugs ($p < 0.05$) and shaded error bars representing SEM. ***C***, % Power change for each drug at the stimulus frequency (±1 Hz), separately for early (100–400 ms, left panel) and late (650–1,750 ms, right panel) stimulus intervals. The solid line represents the mean, and the dashed line represents the median. Significance estimated via cluster-based permutation dependent-sample test indicated by stars (*$p < 0.05$, **$p < 0.01$).

and systematically manipulate the dosage to test for possible effects at higher dosages than the one used here.

Optogenetic manipulations of different interneuron types in animals have established the importance of intracortical inhibition via PV+ interneurons (Bartos et al., 2007, Sohal et al., 2009; Buzsaki and Wang, 2012) as well as SOM+ interneurons (Veit et al., 2017) in the intrinsic generation of gamma-band oscillations. In addition, 40 Hz ASSRs differ from such intrinsically generated gamma-band oscillations in being driven by a temporal modulated stimulus. Yet, it is conceivable, and consistent with our findings, that the inhibitory cortical circuit motifs for the intrinsic generation of gamma-band oscillations are also involved in the resonance in response to an external 40 Hz stimulus. It is however noteworthy that the drive of PV+ cortically projecting interneurons of the basal forebrain can also induce a cortical ASSR (Kim et al., 2015; Hwang et al., 2019), indicating that a GABAergic manipulation may also alter the ASSR via subcortical pathways.

How does a boost of GABAergic synaptic inhibition increase the amplitude of 40 Hz ASSRs in the auditory cortex? Neural circuit modeling has highlighted the importance of the decay time and amplitude of inhibitory postsynaptic currents (IPSC) on PV+ interneurons for the generation of 40 Hz ASSRs (Vierling-Claassen et al., 2008). Other modeling indicates a possible key role of basket cells among PV+ interneurons subtypes in

modulating the amplitude of the response, likely due to their larger number and their different axonal targets compared with chandelier cells (Metzner et al., 2019). Benzodiazepines such as lorazepam increase both IPSC amplitude and decay time (Pawelzik et al., 1999; Kang-Park et al., 2004). In these neural circuit models, those two increases would produce opposing effects on ASSR power. The increase in the 40 Hz ASSR under lorazepam observed in our data is consistent with the IPSC amplitude increase, providing new empirical constraints for circuit models of the 40 Hz ASSR generation.

Different lines of evidence point to an impairment of GABAergic cortical inhibition in schizophrenia. Postmortem studies of schizophrenic patients have revealed a reduction in the GABA transporter GAT-1 (Lewis et al., 2005; Konopaske et al., 2006) and a reduction of GAD-67 (Lewis et al., 2005; Straub et al., 2007), an enzyme responsible of GABA synthesis. This downregulation of inhibitory neurons may be secondary to a deficit in the excitatory drive from pyramidal cells to cortical interneurons (Chung et al., 2016). Indeed, mice lacking NMDA receptors specifically in inhibitory (GABAergic) PV+ interneurons showed a reduced induction of gamma-band oscillations by optogenetic activation, establishing a possible link between NMDA hypofunction, GABAergic downregulation, and cortical gamma oscillations (Carlen et al., 2012). Likewise, magnetic resonance spectroscopic studies of GABA concentrations in
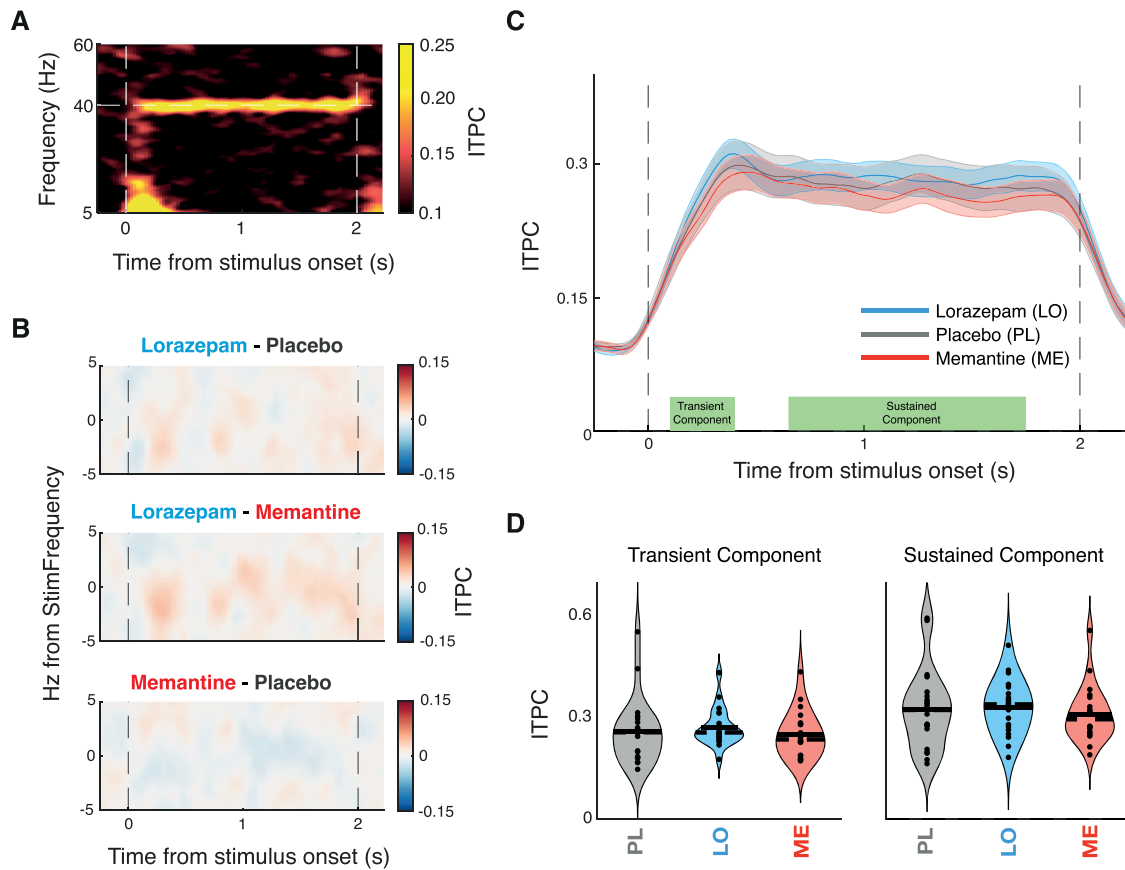
Figure 5. Drug effects on ITPC. ***A***, Time–frequency representation of the ITPC in the early auditory cortex for placebo sessions in which 40 Hz modulated stimuli were presented. ***B***, Time–frequency representation of the drug differences in ITPC in the early auditory cortex. Contour indicating significant differences between drug conditions estimated via Monte Carlo cluster-based permutation dependent-sample t test. The dashed vertical lines indicate stimulus onset and offset. ***B***, ITPC over time averaged across stimulus frequency ±1 Hz for each drug with dots above indicating significant differences between drugs ($p < 0.05$) and shaded error bars representing SEM. ***C***, ITPC for each pharmacological condition at the stimulus frequency (±1 Hz), separately for early (100–400 ms, left panel) and late (650–1,750 ms, right panel) stimulus intervals. The solid line represents the mean, and the dashed line represents the median. Significance estimated via cluster-based permutation dependent-sample test indicated by stars (*$p < 0.05$, **$p < 0.01$).

humans found individual GABA levels to correlate to both peak frequency and amplitude of cortical gamma-band oscillations (Muthukumaraswamy et al., 2009; but see Cousijn et al., 2014) and to be reduced in patients diagnosed with schizophrenia (Yoon et al., 2010, 2020).

One possibility is that the attenuation of 40 Hz ASSRs found in many schizophrenic patients (Kwon et al., 1999; Thune et al., 2016; Tada et al., 2021; Onitsuka et al., 2022) and people at risk of developing schizophrenia (Grent-'t-Jong et al., 2021; Tada et al., 2021) results from a deficit in inhibitory activity of cortical interneurons. Schizophrenia is associated with aberrant, intrinsically generated gamma-band oscillations (Uhlhaas and Singer, 2010; Bianciardi and Uhlhaas, 2021) and has been explained in terms of an imbalance between cortical excitation and inhibition (Foss-Feig et al., 2017). Both intrinsic gamma-band oscillations and cortical excitation–inhibition balance depend critically on intracortical, glutamatergic, and GABAergic transmission. Our finding of a GABAergic transmission modulation of the 40 Hz ASSRs is consistent with these previous ideas.

In conclusion, our results indicate that synaptic inhibition via the GABA$_A$ receptor plays a key role in the generation of the 40 Hz ASSR in the human auditory cortex. Given the established importance of GABAergic inhibition in schizophrenia and other neuropsychiatric disorders, our findings support the utility of

40 Hz ASSR as a noninvasive signature of aberrations of microcircuit-level processes in the human cortex.

References

Bartos M, Vida I, Jonas P (2007) Synaptic mechanisms of synchronized gamma oscillations in inhibitory interneuron networks. Nat Rev Neurosci 8:45–56.

Bastiaansen MC, Knosche TR (2000) Tangential derivative mapping of axial MEG applied to event-related desynchronization research. Clin Neurophysiol 111:1300–1305.

Bianciardi B, Uhlhaas PJ (2021) Do NMDA-R antagonists re-create patterns of spontaneous gamma-band activity in schizophrenia? A systematic review and perspective. Neurosci Biobehav Rev 124:308–323.

Bohorquez J, Ozdamar O (2008) Generation of the 40-Hz auditory steady-state response (ASSR) explained using convolution. Clin Neurophysiol 119:2598–2607.

Buzsaki G, Wang XJ (2012) Mechanisms of gamma oscillations. Annu Rev Neurosci 35:203–225.

Cardin JA, Carlen M, Meletis K, Knoblich U, Zhang F, Deisseroth K, Tsai LH, Moore CI (2009) Driving fast-spiking cells induces gamma rhythm and controls sensory responses. Nature 459:663–667.

Carlen M, et al. (2012) A critical role for NMDA receptors in parvalbumin interneurons for gamma rhythm induction and behavior. Mol Psychiatry 17:537–548.

Chung DW, Fish KN, Lewis DA (2016) Pathological basis for deficient excitatory drive to cortical parvalbumin interneurons in schizophrenia. Am J Psychiatry 173:1131–1139.

Cousijn H, Haegens S, Wallis G, Near J, Stokes MG, Harrison PJ, Nobre AC (2014) Resting GABA and glutamate concentrations do not predict

visual gamma frequency or amplitude. Proc Natl Acad Sci U S A 111: 9301–9306.

Donner TH, Siegel M (2011) A framework for local cortical oscillation patterns. Trends Cogn Sci 15:191–199.

Foss-Feig JH, Adkinson BD, Ji JL, Yang G, Srihari VH, McPartland JC, Krystal JH, Murray JD, Anticevic A (2017) Searching for cross-diagnostic convergence: neural mechanisms governing excitation and inhibition balance in schizophrenia and autism spectrum disorders. Biol Psychiatry 81:848–861.

Galambos R, Makeig S, Talmachoff PJ (1981) A 40-Hz auditory potential recorded from the human scalp. Proc Natl Acad Sci U S A 78:2643–2647.

Glasser MF, et al. (2016) A multi-modal parcellation of human cerebral cortex. Nature 536:171–178.

Gramfort A, et al. (2013) MEG and EEG data analysis with MNE-Python. Front Neurosci 7:267.

Greenblatt DJ, Divoll M, Harmatz JS, Shader RI (1982) Pharmacokinetic comparison of sublingual lorazepam with intravenous, intramuscular, and oral lorazepam. J Pharm Sci 71:248–252.

Grent-'t-Jong T, Gajwani R, Gross J, Gumley AI, Krishnadas R, Lawrie SM, Schwannauer M, Schultze-Lutter F, Uhlhaas PJ (2021) 40-Hz auditory steady-state responses characterize circuit dysfunctions and predict clinical outcomes in clinical high-risk for psychosis participants: a magnetoencephalography study. Biol Psychiatry 90:419–429.

Grent-'t-Jong T, Brickwedde M, Metzner C, Uhlhaas PJ (2023) 40- Hz auditory steady state responses in schizophrenia: towards a mechanistic biomarker for circuit dysfunctions and early detection and diagnosis. Biol Psychiatry 94:550–560.

Hong LE, Summerfelt A, McMahon R, Adami H, Francis G, Elliott A, Buchanan RW, Thaker GK (2004) Evoked gamma band synchronization and the liability for schizophrenia. Schizophr Res 70:293–302.

Hwang E, Brown RE, Kocsis B, Kim T, McKenna JT, McNally JM, Han HB, Choi JH (2019) Optogenetic stimulation of basal forebrain parvalbumin neurons modulates the cortical topography of auditory steady-state responses. Brain Struct Funct 224:1505–1518.

Jadi MP, Behrens MM, Sejnowski TJ (2016) Abnormal gamma oscillations in N-methyl-D-aspartate receptor hypofunction models of schizophrenia. Biol Psychiatry 79:716–726.

Jefsen OH, Shtyrov Y, Larsen KM, Dietz MJ (2022) The 40-Hz auditory steady-state response in bipolar disorder: a meta-analysis. Clin Neurophysiol 141:53–61.

Johnson JW, Kotermanski SE (2006) Mechanism of action of memantine. Curr Opin Pharmacol 6:61–67.

Kang-Park MH, Wilson WA, Moore SD (2004) Differential actions of diazepam and zolpidem in basolateral and central amygdala nuclei. Neuropharmacology 46:1–9.

Kienitz R, et al. (2022) Benzodiazepines in the management of seizures and status epilepticus: a review of routes of delivery, pharmacokinetics, efficacy, and tolerability. CNS Drugs 36:951–975.

Kim T, et al. (2015) Cortically projecting basal forebrain parvalbumin neurons regulate cortical gamma band oscillations. P Natl Acad Sci USA 112:3535–3540.

Konopaske GT, Sweet RA, Wu Q, Sampson A, Lewis DA (2006) Regional specificity of chandelier neuron axon terminal alterations in schizophrenia. Neuroscience 138:189–196.

Kwon JS, O'Donnell BF, Wallenstein GV, Greene RW, Hirayasu Y, Nestor PG, Hasselmo ME, Potts GF, Shenton ME, McCarley RW (1999) Gamma frequency-range abnormalities to auditory stimulation in schizophrenia. Arch Gen Psychiatry 56:1001–1005.

Lewis DA, Hashimoto T, Volk DW (2005) Cortical inhibitory neurons and schizophrenia. Nat Rev Neurosci 6:312–324.

Light GA, Zhang W, Joshi YB, Bhakta S, Talledo JA, Swerdlow NR (2017) Single-dose memantine improves cortical oscillatory response dynamics in patients with schizophrenia. Neuropsychopharmacology 42:2633–2639.

Metzner C, Zurowski B, Steuber V (2019) The role of parvalbumin-positive interneurons in auditory steady-state response deficits in schizophrenia. Sci Rep 9:18525.

Munch AS, Amat-Foraster M, Agerskov C, Bastlund JF, Herrik KF, Richter U (2023) Sub-anesthetic doses of ketamine increase single cell entrainment in the rat auditory cortex during auditory steady-state response. J Psychopharmacol 37:822–835.

Muthukumaraswamy SD, Edden RA, Jones DK, Swettenham JB, Singh KD (2009) Resting GABA concentration predicts peak gamma frequency

and fMRI amplitude in response to visual stimulation in humans. Proc Natl Acad Sci U S A 106:8356–8361.

Noetzli M, Eap CB (2013) Pharmacodynamic, pharmacokinetic and pharmacogenetic aspects of drugs used in the treatment of Alzheimer's disease. Clin Pharmacokinet 52:225–241.

Onitsuka T, Tsuchimoto R, Oribe N, Spencer KM, Hirano Y (2022) Neuronal imbalance of excitation and inhibition in schizophrenia: a scoping review of gamma-band ASSR findings. Psychiatry Clin Neurosci 76:610–619.

Oostenveld R, Fries P, Maris E, Schoffelen JM (2011) Fieldtrip: open source software for advanced analysis of MEG, EEG, and invasive electrophysiological data. Comput Intell Neurosci 2011:156869.

Ozdamar O, Bohorquez J, Ray SS (2007) P(b)(P(1)) resonance at 40 Hz: effects of high stimulus rate on auditory middle latency responses (MLRs) explored using deconvolution. Clin Neurophysiol 118:1261–1273.

Pastor MA, Artieda J, Arbizu J, Marti-Climent JM, Penuelas I, Masdeu JC (2002) Activation of human cerebral and cerebellar cortex by auditory stimulation at 40 Hz. J Neurosci 22:10501–10506.

Pawelzik H, Bannister AP, Deuchars J, Ilia M, Thomson AM (1999) Modulation of bistratified cell IPSPs and basket cell IPSPs by pentobarbitone sodium, diazepam and Zn:: dual recordings in slices of adult rat hippocampus. Eur J Neurosci 11:3552–3564.

Plourde G, Baribeau J, Bonhomme V (1997) Ketamine increases the amplitude of the 40-Hz auditory steady-state response in humans. Br J Anaesth 78:524–529.

Presacco A, Bohorquez J, Yavuz E, Ozdamar O (2010) Auditory steady-state responses to 40-Hz click trains: relationship to middle latency, gamma band and beta band responses studied with deconvolution. Clin Neurophysiol 121:1540–1550.

Rass O, Forsyth JK, Krishnan GP, Hetrick WP, Klaunig MJ, Breier A, O'Donnell BF, Brenner CA (2012) Auditory steady state response in the schizophrenia, first-degree relatives, and schizotypal personality disorder. Schizophr Res 136:143–149.

Ross B, Picton TW, Pantev C (2002) Temporal integration in the human auditory cortex as represented by the development of the steady-state magnetic field. Hearing Res 165:68–84.

Ross B, Herdman AT, Pantev C (2005) Right hemispheric laterality of human 40 Hz auditory steady-state responses. Cereb Cortex 15:2029–2039.

Sivarao DV, Chen P, Senapati A, Yang Y, Fernandes A, Benitex Y, Whiterock V, Li YW, Ahlijanian MK (2016) 40 Hz auditory steady-state response is a pharmacodynamic biomarker for cortical NMDA receptors. Neuropsychopharmacology 41:2232–2240.

Sivarao DV, Frenkel M, Chen P, Healy FL, Lodge NJ, Zaczek R (2013) MK-801 disrupts and nicotine augments 40 Hz auditory steady state responses in the auditory cortex of the urethane-anesthetized rat. Neuropharmacology 73:1–9.

Sohal VS, Zhang F, Yizhar O, Deisseroth K (2009) Parvalbumin neurons and gamma rhythms enhance cortical circuit performance. Nature 459:698–702.

Straub RE, Lipska BK, Egan MF, Goldberg TE, Callicott JH, Mayhew MB, Vakkalanka RK, Kolachana BS, Kleinman JE, Weinberger DR (2007) Allelic variation in GAD1 (GAD67) is associated with schizophrenia and influences cortical function and gene expression. Mol Psychiatry 12:854–869.

Sullivan EM, Timi P, Hong LE, O'Donnell P (2015) Effects of NMDA and GABA-A receptor antagonism on auditory steady-state synchronization in awake behaving rats. Int J Neuropsychopharmacol 18:pyu118.

Tada M, et al. (2021) Global and parallel cortical processing based on auditory gamma oscillatory responses in humans. Cereb Cortex 31:4518–4532.

Tan HR, Gross J, Uhlhaas PJ (2015) MEG-measured auditory steady-state oscillations show high test-retest reliability: a sensor and source-space analysis. Neuroimage 122:417–426.

Thune H, Recasens M, Uhlhaas PJ (2016) The 40-Hz auditory steady-state response in patients with schizophrenia: a meta-analysis. JAMA Psychiatry 73:1145–1153.

Uhlhaas PJ, Singer W (2010) Abnormal neural oscillations and synchrony in schizophrenia. Nat Rev Neurosci 11:100–113.

Van Veen BD, van Drongelen W, Yuchtman M, Suzuki A (1997) Localization of brain electrical activity via linearly constrained minimum variance spatial filtering. IEEE Trans Biomed Eng 44:867–880.

Veit J, Hakim R, Jadi MP, Sejnowski TJ, Adesnik H (2017) Cortical gamma band synchronization through somatostatin interneurons. Nat Neurosci 20:951–959.

Vierling-Claassen D, Siekmeier P, Stufflebeam S, Kopell N (2008) Modeling GABA alterations in schizophrenia: a link between impaired inhibition and altered gamma and beta range auditory entrainment. J Neurophysiol 99:2656–2671.

Vohs JL, Chambers RA, Krishnan GP, O'Donnell BF, Berg S, Morzorati SL (2010) GABAergic modulation of the 40 Hz auditory steady-state response in a rat model of schizophrenia. Int J Neuropsychopharmacol 13:487–497.

Vohs JL, Chambers RA, O'Donnell BF, Krishnan GP, Morzorati SL (2012) Auditory steady state responses in a schizophrenia rat model probed by excitatory/inhibitory receptor manipulation. Int J Psychophysiol 86: 136–142.

Wang X, Li Y, Chen J, Li Z, Li J, Qin L (2020) Aberrant auditory steady-state response of awake mice after single application of the NMDA receptor antagonist MK-801 into the medial geniculate body. Int J Neuropsychopharmacol 23:459–468.

Wilming N, Murphy PR, Meyniel F, Donner TH (2020) Large-scale dynamics of perceptual decision information across human cortex. Nat Commun 11:5109.

Wilson TW, Rojas DC, Reite ML, Teale PD, Rogers SJ (2007) Children and adolescents with autism exhibit reduced MEG steady-state gamma responses. Biol Psychiatry 62:192–197.

Yamazaki M, Honda S, Tamaki K, Irie M, Mihara T (2020) Effects of (+)-bicuculline, a GABAa receptor antagonist, on auditory steady state response in free-moving rats. PLoS One 15:e0236363.

Yoon JH, Maddock RJ, Rokem A, Silver MA, Minzenberg MJ, Ragland JD, Carter CS (2010) GABA concentration Is reduced in visual cortex in schizophrenia and correlates with orientation-specific surround suppression. J Neurosci 30:3777–3781.

Yoon JH, Maddock RJ, DongBo Cui E, Minzenberg MJ, Niendam TA, Lesh T, Solomon M, Ragland JD, Carter C (2020) Reduced in vivo visual cortex GABA in schizophrenia, a replication in a recent onset sample. Schizophr Res 215:217–222.